Journal of Materials Chemistry A

PAPER

View Article Online
View Journal | View Issue

Cite this: J. Mater. Chem. A, 2018, 6, 22301

Terahertz short-range mobilities in neat and intermixed regions of polymer:fullerene blends with controlled phase morphology†

Philipp Krauspe,[a] Demetra Tsokkou,[a] Martina Causa',[a] Ester Buchaca-Domingo,[b] Zhuping Fei,[b] Martin Heeney,[b] Natalie Stingelin[bc] and Natalie Banerji *[a]

The molecular-level arrangement of the donor and acceptor (*i.e.* the local morphology) in organic solar cells governs charge separation and charge transport *via* its effect on the mobility of charges. However, the nanometre-scale mobility in such systems, which can be measured using terahertz (THz) spectroscopy, has been little investigated at relevant low excitation densities, due to extremely weak signals. Here, we study the mobility over short distances and at ultrashort times using time-resolved optical-pump-THz-probe (OPTP) spectroscopy on pBTTT:PCBM blends. This complements our previous results obtained with transient absorption (TA) and electro-modulated differential absorption (EDA) techniques. In the pBTTT:PCBM system, the co-existence of fullerene-/polymer-rich ('neat') and co-crystalline ('intermixed') regions can be controlled through choice of composition (weight ratio of the two components, use of processing additive). We demonstrate high short-range mobilities that help charges separate, and we show how this mobility of photogenerated charges develops in time, in particular as the charges move between different phase regions of the blend. By reducing the pump fluence below the threshold for nonlinear recombination mechanisms, we access these properties at solar cell operating conditions. Overall, we explain the necessity of different local phases through their influence on charge lifetime and mobility.

Received 19th August 2018
Accepted 9th October 2018

DOI: 10.1039/c8ta08061e

rsc.li/materials-a

Introduction

Record power conversion efficiencies in state-of-the-art organic solar cells based on conjugated polymer electron donors blended with fullerene acceptors reach 10.6%,[1] while polymer:NFA (non-fullerene acceptor) systems with 13% performance have recently been reported.[2] Other advantages of using lead-free organic materials for photovoltaics include low-cost manufacturing, flexibility, light-weight, tunability and relatively good stability.[3–5] The transport properties of electrons and holes in the organic semiconductor thin films play a primordial role in ensuring that charges reach the electrodes instead of recombining and hence govern the photovoltaic performance. Understanding transport in such materials is however challenging, since the accessible mobility of charges depends on the distance and time scale over which it is probed.[6–9] For instance, charge transport is known to be highly dispersive: fast and highly mobile charges are found on the local (<10 nm) length scale along well-ordered polymer backbone segments, while the long-range mobility over hundreds of nanometres to micrometre distances is orders of magnitude lower, since deviations from the crystalline packing, the lack of tie molecules, grain boundaries, and other structural defects can lead to a drastic reduction in charge mobility.[10] It has indeed been shown that charges travel preferentially along polymer backbones and jump between chains in locally well-packed aggregates.[11] It is therefore crucial to investigate the short-range mobilities and their dependence on phase morphology.[12]

A second reason why short-range charge mobility in organic semiconductors is important is its impact on charge generation in bulk heterojunction solar cells. Short-range mobility has been put forward to be one of the factors (together with presence of an energy cascade, charge delocalization, entropy effects *etc.*) that allows charge separation at donor:acceptor interfaces.[13,14] When introducing short-range mobilities (rather than long-range ones) in Kinetic Monte Carlo simulations, the increased number of splitting attempts of geminate electron–hole pairs was proposed to lead to a higher probability of the charges separating instead of recombining.[8] Charge separation also critically depends on the nanoscale structure and phase morphology at the interface, since the ensuing energetic

[a]Department of Chemistry and Biochemistry, University of Bern, Freiestrasse 3, 3012 Switzerland. E-mail: natalie.banerji@dcb.unibe.ch

[b]Centre for Plastic Electronics, Imperial College London, Exhibition Road, London, SW7 2AZ, UK

[c]School of Materials Science & Engineering, School of Chemical & Biomolecular Engineering, Georgia Institute of Technology, Atlanta, Georgia 30332, USA

† Electronic supplementary information (ESI) available. See DOI: 10.1039/c8ta08061e

landscape can make it favourable for charges to separate. For example, the co-existence of relatively phase-pure ('neat') polymer and fullerene domains with intermixed polymer:fullerene regions creates advantageous energy cascades. The local morphology also limits the extent over which the charges can delocalize; intimate mixing of the donor and acceptor can for instance reduce the charge separation distance and thus hinder the escape from geminate recombination.[9,15] We expect that the local structure and the different phase domains in polymer:fullerene blends also impact the short-range charge mobility, but this has to our knowledge not yet been investigated.

While several techniques exist to measure long-range charge transport (time of flight, carrier extraction by linearly increasing voltage, impedance spectroscopy, transistor measurements), only microwave-conductivity or terahertz (THz) spectroscopy allow to evaluate the short-range transport properties of charges, and this without contacting the active layer. Spectroscopy in the THz (10^{12} Hz) range accesses the transport of charges within the THz pulse oscillating electric field of 1 ps. That results in measuring short-range charge motion on length scales on the order of a few nanometres, relevant to the local phase morphology of polymer:fullerene blends. Moreover, only THz spectroscopy provides the opportunity to follow the conductivity of photogenerated charges with picosecond resolution following photoexcitation in optical-pump-THz-probe (OPTP) measurements, while microwave-conductivity techniques are limited to nanosecond time resolution. This high time resolution is important in order to follow the evolution of the short-range mobility on the time scale that the charges evolve between the different phases of the investigated polymer:fullerene blends. Early OPTP studies on organic semiconductors concentrated on comparisons of different polymers and their associated performance as a solar cell material.[16,17] The technique has also been used to investigate charges within P3HT:PCBM blends and their dependence on temperature (exciting either the polymer or the fullerene),[18] to study molecular packing effects by comparing charges in films to solutions,[19] to investigate the influence of regioregularity of the polymer to the conductivity,[20] or to investigate the mobilities of holes and electrons separately.[21] However, with a few exceptions,[22] most previous OPTP studies where carried out at orders of magnitude higher excitation fluences than the ones encountered under solar illumination, making a direct comparison to photovoltaic device properties difficult. Indeed, sampling the OPTP response with pump fluences varied over four orders of magnitude revealed prominent non-linear processes (carrier–carrier scattering or bimolecular recombination).[23]

Thus, although the importance of short-range charge mobility in organic solar cell materials has been recognized and THz spectroscopy provides the ideal technique to investigate it, there exists to date no systematic investigation linking the short-range THz mobility to the local phase-morphology of the blends, at relevant low pump fluences. Here, we have therefore carried out an OPTP study on pBTTT:PCBM model systems, where the phase morphology has been precisely characterized and can be controlled.[24,25] Accepting the challenging low signal intensities, we have carried out all measurements at low fluences. This did not only allow to perform measurements that are relevant to solar cell conditions, but also to directly compare our findings to transient absorption (TA) and electro-modulated differential absorption (EDA) measurements that we had previously carried out on those systems.[25–29] The former allowed us to determine the dynamics of the charge population, while the latter (a technique related to TREFISH[30]) provided the possibility to follow the average distance between electrons and holes as they drift apart in an electric field, yielding short-range mobilities at ultrafast times and increasingly long-range mobilities at longer times. The OPTP experiments give access to valuable complementary short-range mobilities of the charges at different times following photo-excitation, thus tracking their short-range mobilities as they evolve between different phases of the blends regardless of the distance that they have travelled since their generation. We thus gain unique insights about the effects of the phase-morphology on the interplay of different short-range mobilities that govern charge transport and charge separation in bulk heterojunction organic solar cells.

Methods

Sample preparation

The synthesis of poly(2,5-bis(3-hexadecyl-thiophen-2-yl)thieno[3,2-*b*]thiophene) (pBTTT, $M_n = 34$ kDa, $M_w = 66$ kDa, chemical structure in Fig. S1a†), as used in this study, has been previously reported.[31] We purchased [6,6]-phenyl C_{61} butyric acid methyl ester (PCBM) from Solenne, and the heptanoic acid methyl ester (Me7) additive from Aldrich. They were used without further purification. As reported in detail elsewhere,[25,32] we prepared solutions of pBTTT : PCBM (1 : 1 or 1 : 4 weight ratio) in 1,2-*ortho*-dichlorobenzene. For the 1 : 1 pBTTT:PCBM blend processed with Me7, we added 10 molar equivalents of the additive per monomer unit of the polymer to the solution. The concentration of pBTTT was 10 mg mL^{-1} in all solutions, which we left stirring for more than 4 hours at 100 °C to ensure complete dissolution of the materials. We then deposited films of about 1 μm thickness by drop-casting from hot solutions (~85 °C) onto z-cut quartz substrates kept at either room temperature (Me7 sample) or 35 °C (1 : 1 and 1 : 4 blends).

Optical-pump-THz-probe spectroscopy

The optical-pump-terahertz-probe (OPTP) setup was based on the output of a regeneratively-amplified Ti:sapphire laser system with an average output power of 6 mJ at 800 nm, with ~35 fs pulse duration at 1 kHz repetition rate (Coherent Astrella). Part of the beam entered an optical parametric amplifier (OPA, Coherent Opera Solo), whose output at 540 nm was used as the pump. The second pump option at 400 nm was generated by second harmonic generation in a BBO crystal. The photoexcited samples were probed by THz pulses, which were generated *via* optical rectification in a 2 mm [110] ZnTe crystal. Peak electric fields were around 2 kV cm^{-1}. The THz probe and optical pump pulses were spatially overlapped on the sample.

The THz probe pulse was subsequently detected using electro-optic sampling in another 1 mm [110] ZnTe crystal. The OPTP measurements were done in N_2 atmosphere to avoid oxidation of the samples and absorption of the THz beam by moisture. Two different measurement modes were employed: (1) varying the pump–probe time delay by shifting the pump beam in time while scanning with the peak THz probe electric field yielded the photoconductivity dynamics. (2) Scanning the THz probe beam at a given pump–probe time delay measured the frequency-dependent instantaneous response of the THz field to the charges within the excited material and yielded the frequency-dependent photoconductivity spectrum at given pump–probe time delay.

Results and discussion

Photoconductivity dynamics in 1 : 1 and 1 : 4 pBTTT:PCBM blends

One way that we selected to manipulate the phase morphology of the pBTTT:PCBM blends was to vary the polymer : fullerene ratio. PCBM intercalates between the sidechains of pBTTT in the 1 : 1 blend (by weight) yielding a highly intermixed co-crystal phase, while the excess PCBM in the 1 : 4 blend forms fullerene-rich clusters in addition to the co-crystalline polymer:fullerene regions (schematic representation in Fig. S1b and c†).[24,26,33] In devices, the 1 : 4 blend shows higher solar cell efficiency than the 1 : 1 blend, due to the beneficial impact of the fullerene-rich domains.[24,34] The time evolution of the photoconductivity (measured at the peak THz field) upon excitation at 540 nm of the 1 : 1 (top) and 1 : 4 (bottom) systems is shown in Fig. 1. At this wavelength, predominantly the pBTTT is excited. The photoconductivity dynamics reflects the absorption of the THz pulse by the photogenerated charges, which is related to their short-range mobility, their density and their delocalization, including localization effects of the immediate surroundings of the charges (see discussion of the modified Drude model, below). In previous THz studies of organic semiconductors, ultrafast decays of around 0.5–5 ps have been observed, which we can suppress by reducing the excitation density below the threshold of nonlinear recombination, such as carrier–carrier scattering and bimolecular recombination.[23] Indeed, a sufficiently low fluence ensures that the material systems are probed closer to device operating conditions (see Fig. S2†), at the cost of less signal intensity leading to more noise. Reassuringly, despite the noise, we find significant differences between samples of different phase morphologies and excitation wavelengths, while the number of exciting photons was kept constant at 1.14×10^{13} photons per cm^2. We are confident that we are below the threshold of nonlinear recombination effects because the data is in good agreement with population dynamics obtained from TA measurements at low fluences.

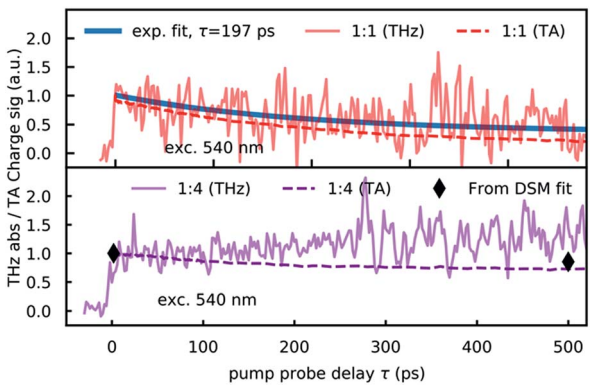

Fig. 1 THz photoconductivity dynamics on the one-phase 1 : 1 blend only comprising co-crystalline regions (top) and a two-phase system with additional PCBM-rich regions (1 : 4) (bottom), excited with optical pump pulses of 540 nm at 1.14×10^{13} photons per cm^2. Solid lines show the absorption of the maximum THz field at varied pump–probe delays. Dashed lines show the charge population extracted from TA measurements. Black diamonds in the lower panel show the normalized charge density extracted from fits of the Drude–Smith model to frequency-dependent photoconductivity spectra at pump-probe time delays of +2 and at +500 ps, respectively.

For both systems, we find that charges are formed within a time scale shorter than our instrument resolution (100 fs) leading to the instantaneous rise in photoconductivity (Fig. 1). This is in agreement with our previous TA measurements, which revealed ultrafast electron transfer (ET) when pBTTT in the intermixed regions is excited in the 1 : 1 or 1 : 4 blends.[26,32] The TA charge population dynamics, which are shown as dashed lines in Fig. 1, indicate that in the 1 : 1 sample with 540 nm excitation, 87% of photogenerated charges undergo geminate recombination (gCR) with a time constant of 200 ps. The THz photoconductivity dynamics closely follows this trend, showing that the THz response is dominated by the charge population. Indeed, as some charges undergo gCR, this leads to a decay in the charge density and thus reduces the measured THz conductivity in the 1 : 1 blend. In the THz photoconductivity dynamics, we observe this decay (fit with a single exponential function with a time constant of 197 ps), as in the TA data. The same measurement performed on the 1 : 4 sample shows a slight rise in the THz absorption, while there is a slight 200 ps decay in the TA charge population dynamics due to gCR. The decay of the charge density (about 30%) in samples with excess PCBM is weaker than in the 1 : 1 blend, due to electrons migrating to the PCBM-rich regions, which has a beneficial effect on the spatial separation of charges.[26,33,34] This has also been observed in P3HT:PCBM blends, explaining the superior solar cell performance of blends with excess PCBM.[35] The discrepancy between the TA pure population dynamics and the THz photoconductivity dynamics, which represent a population-mobility product, suggest changes in the short-range effective mobility of the charges as they evolve from the intercalated regions to the PCBM-rich regions after charge separation in the 1 : 4 blend. We conclude that the mobility and localization of individual charges is affected by the local phase composition. This change is not observed in the 1 : 1 blend, where only one phase is present and charges cannot migrate between different phases.

Fig. 2 shows the time evolution of the THz photoconductivity for measurements with pump pulses at 400 nm, where pBTTT is excited with excess energy and PCBM also considerably absorbs.

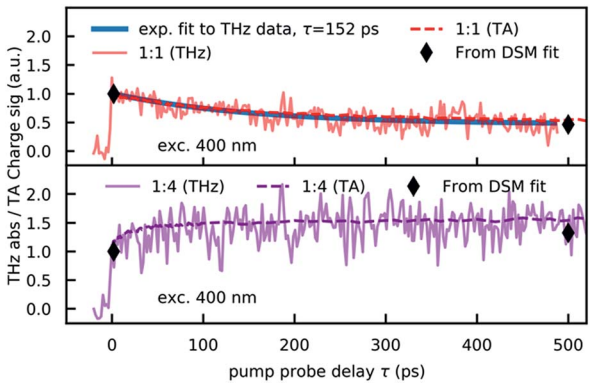

Fig. 2 THz photoconductivity dynamics on the 1 : 1 blend (top) and the two-phase-system with additional PCBM-rich regions (1 : 4) (bottom), excited with optical pump pulses of 400 nm at 1.14×10^{13} photons per cm^2. Solid lines show the absorption of the maximum THz field at varied pump–probe delays. Dashed lines show the charge population extracted from TA measurements. Black diamonds in the lower panel show the normalized charge density extracted from fits of the Drude–Smith model to frequency-dependent photoconductivity spectra at pump–probe time delays of +2 and at +500 ps, respectively.

In the one-phase co-crystalline 1 : 1 sample, we find a decay of the THz absorption signal with pump–probe delay which closely follows the charge signature of the TA measurements and presents a pronounced gCR component with a 152 ps time constant. As we have previously reported,[26] the charge population dynamics is comparable to the one at 540 nm excitation, even if part of the charges are now generated by ultrafast hole transfer (HT) following excitation of PCBM in the co-crystalline regions. The extent of gCR drops however from 87% to 75% with 400 nm excitation (Fig. S3†). From the similarity of the TA and THz dynamics in the 1 : 1 blend at 400 nm, we conclude again that the photoconductivity is dominated by the charge density. In the 1 : 4 system with PCBM-rich regions, exciting with 400 nm pulses also generates excitons in these fullerene domains. The excitons first need to diffuse to the intermixed regions before undergoing delayed HT. This leads to the rise over the first 50 ps in our THz conductivity data. PCBM excitons that reach the co-crystalline phase are split and can be separated spatially with the electrons occupying PCBM-rich regions and holes travelling along the polymer backbones into the co-crystalline region. We have recently shown that significant electric fields must be applied *via* external electrodes to generate free charges in neat C_{60} and PCBM films, so that we exclude here direct generation of charges in the PCBM-rich regions due to the very weak THz probe beam.[36] The charge population derived from TA measurements is shown as dashed lines in Fig. 2. We find compelling agreement of THz absorption and the time evolution of charges hinting at no significant change in the effective mobilities.

Photoconductivity spectra of the 1 : 1 and 1 : 4 pBTTT:PCBM blends

Instead of focusing only on the THz absorption at the THz field maximum, we also performed frequency-dependent studies of the THz conductivity. As described below, analysis of this data gives more thorough information about the absorption and dispersion that the THz pulse undergoes in the photoexcited sample, yielding insights about the nature, short-range mobility and density of the charges. We have analyzed the complex frequency-dependent photoconductivity $\sigma(\tau)$ at two distinct pump–probe time delays: $\tau = 2$ ps and $\tau = 500$ ps, respectively. The complex photoconductivity spectra are calculated from the Fourier transform of the response of the THz probe pulse to the non-excited sample and the Fourier transform of differential transmission of the THz pulse with and without excitation.[37] From these, the real and imaginary parts of the spectra are extracted and shown in Fig. 3. The real part of the measured photoconductivity spectra is shown with square symbols, while the imaginary part is shown using circles for the 1 : 1 co-crystal system and the 1 : 4 blend with PCBM-rich regions. The imaginary part being negative (zero at low frequency and decreasing at higher frequencies) is a typical signature of dispersive transport of somewhat bound charges.[38] Therefore, the real and imaginary parts of each set were fit with the modified Drude–Smith Model (DSM), which is well established for the description of charge carriers in disordered media that exhibit localization on a length scale corresponding to several monomer units in conjugated polymers:

$$\tilde{\sigma}(\omega) = \frac{\varepsilon_0 {\omega_p}^2 \tau}{1 - i\omega\tau}\left[1 + \frac{c_1}{1 - i\omega\tau}\right]$$

Here, the plasma frequency squared, ${\omega_p}^2 = ne^2/\varepsilon_0 m_e$, scales with the charge density n. The result of this fitting parameter is represented with black diamonds in Fig. 1 and 2, normalized at short times. The excellent agreement with the TA population dynamics is a clear indication of the robustness of our analysis, in spite of the noisy data at low excitation fluences. Moreover, the scattering time τ in the model can be connected to the THz mobility *via* $\mu_{THz} = e\tau/m^*$. The effective mass $m^* = 1.7m_e$ of the charges in our systems is assumed to be similar to P3HT:PCBM blends, since P3HT and PBTTT have the same m^*.[39] The THz mobility can be considered as resulting from very local (few

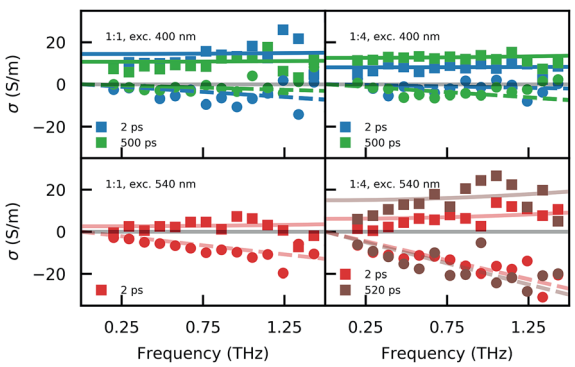

Fig. 3 Complex photoconductivity spectra (squares for the real part and circles for the imaginary part) and Drude–Smith model fits (solid lines) for the 1 : 1 and the 1 : 4 systems at 400 nm and 540 nm excitation show the difference of the short range mobility at a pump–probe delay of +2 ps *versus* +500 ps. Fit results and a detailed description of the model are found in the main text.

nanometre) ballistic transport in polymer chain segments or local aggregates over which the charges can delocalize. The extent of delocalization is typically limited in organic semiconductors, for example due to the finite polymer chain length, disorder, or coupling of electronic states to nuclear modes.[40–42] This localization leads to energy barriers and backscattering in the transport, which therefore occurs by incoherent hopping of the charges even on a relatively short length scale. In the DSM, this is described by the localization parameter c_1. It ranges from $c_1 = -1$ for perfect backscattering at boundaries, to $c_1 = 0$ which recovers the unperturbed Drude model. In the case of organic semiconductors, this measure of localization can be interpreted as how weakly bound charges are. Perfect backscattering is expected for charges that are trapped on a short polymer segment without sufficient delocalization over extended π-orbitals. Since the THz mobilities calculated from the scattering times inside the DSM ignore the localization, we introduce the effective THz mobility as $\mu_{\text{eff}} = \mu_{\text{THz}}(1 + c_1)$.[38]

We note that the effective mobilities obtained in our THz experiments still correspond to a short-range mobility and therefore differ from true DC mobilities measured from time of flight or transistor measurements that involve longer length scales dominated *e.g.* by grain boundaries. Charges travel at their drift velocity $v_D = \mu E$, with E being the applied electric field. In our experiments, this field is on the order of 2 kV cm^{-1}, leading to drift velocities of nm ps^{-1}. Since the period of the probing THz electric field is close to 1 ps, we probe the charges on the nanometre length scale and therefore at the length scale of local phase environments. Another aspect of our THz measurement geometry is that the probed sample area is on the order of 1 mm. Therefore, we cannot selectively target local phases, but average over all domains and defects when calculating the effective values for the delocalization and scattering times. Finally, it is not possible to distinguish between hole and electron mobility, because there is no selectivity between them in THz spectroscopy. In a previous report, the authors varied the molecular weight of the polymer or used the equivalent monomer and showed that typically the hole mobility is higher and therefore dominates the THz response in polymer:PCBM blends.[21]

Table 1 shows the fit results obtained with the DSM, including the effective mobilities. For the 1 : 1 one-phase-sample, we find that at short times (2 ps) after photoexcitation, the THz mobility is similar at 400 nm and 540 nm excitation (comparable scattering times), while the effective mobility differs due to the stronger localization when exciting at 540 nm. In this case, exciting with higher excess energy leads to slightly more delocalization consistent with previous studies of more localized charges closer to the band gap. The underlying mechanism is the stronger influence of vibrations on states closer to the cut-off in the density of states.[43] Comparing the plasma frequencies at 2 ps we find significantly more charge population when exciting at 540 nm, simply because the sample absorbs more at this wavelength and we used similar pump fluences.[32] A determination of the precise yield of charge carriers is however not possible since we could not account for losses due to reflection and residual transmission of the pump. At a longer time delay of 500 ps, most charges in the 1 : 1 blend have recombined due to gCR (see strong reduction in the plasma frequency), explaining why the photoconductivity dynamics are dominated by the charge density in Fig. 1 and 2. Considering the DSM parameters for the 1 : 1 blend excited at 400 nm in Table 1, it is moreover obvious that the localization parameter significantly decreases over time, and that both the terahertz and effective mobilities increase. This shows that the small population of charges that can separate and does not undergo gCR, in spite of the strong intermixing of the donor and acceptor, is characterized by a particularly high short-range mobility and delocalization. This is facilitated by the high local order that is present in the co-crystalline regions of pBTTT:PCBM blends, where fullerenes intercalate in a regular fashion in the polymer sidechains. The high short-range mobility stems likely from holes on the polymer backbones. This is because in this system electrons cannot delocalize over many fullerenes, since there are no fullerene-rich regions available.

For the two-phase 1 : 4 sample containing co-crystalline regions as well as fullerene-rich clusters, we observe a similar strong localization (and only slightly higher THz mobility) as in the 1 : 1 blend, 2 ps after exciting the polymer in the intercalated regions at 540 nm (Table 1). At longer time delays, there is a slight decrease in the localization parameter and increase in the THz mobility, leading to an overall increase in the effective mobility. This justifies the deviation of the THz photoconductivity dynamics from the TA and DSM population dynamics, which reflect only the slight decrease in charge density due to gCR (Fig. 1). The increase in the short-range mobility is due to a combination of those charges not undergoing gCR having a higher mobility, and of electrons reaching the PCBM-rich clusters, which occurs on the tens of ps time scale.[26] We find initially more delocalized charges when exciting the 1 : 4 blend with 400 nm pulses, but a THz mobility similar to the 1 : 1 systems (Table 1). The higher delocalization is due to both the excess energy and the fact that a significant fraction of the excitation occurs in PCBM-rich domains. This implies that upon exciton splitting at the interface between fullerene rich and co-crystalline regions, the electrons are directly formed in the fullerene-rich clusters and not within the intermixed domains. When going to 500 ps for the 1 : 4 blend with 400 nm excitation, we notice a relatively small evolution of the effective mobility, as most of the electrons and holes are already separated between the PCBM-rich and the co-crystalline regions from early times on. Therefore, the THz photoconductivity dynamics (Fig. 2) is dominated by the charge population, namely their increase due to delayed HT. In general, we find comparable THz mobilities in the 1 : 1 and 1 : 4 systems and at both excitation energies at the long 500 ps time delay. The differences in the photoconductivity that we observed in the THz dynamics stem therefore from the charge density and their localization, which are strongly dependent on the phase morphology.

Photoconductivity dynamics and spectra in a partially phase-separated 1 : 1 pBTTT:Me7:PCBM blend

So far, we have discussed the role of co-crystalline regions and PCBM-rich clusters. To further investigate the influence of the

Table 1 Fit results of the modified DSM on the frequency-dependent photoconductivity of the 1 : 1 and 1 : 4 blends at 400 nm and 540 nm excitation

	540 nm	c_1	τ [fs]	μ_{THz} [cm^2 V^{-1} s^{-1}]	μ_{eff} [cm^2 V^{-1} s^{-1}]	$\omega_p{}^2$ [THz]
1 : 1	2 ps	−0.99	26.0	26.3	0.3	39.9
1 : 4	2 ps	−0.98	36.0	36.4	0.7	40.3
	500 ps	−0.95	45.2	45.7	2.3	34.4
	400 nm	c_1	τ [fs]	μ_{THz} [cm^2 V^{-1} s^{-1}]	μ_{eff} [cm^2 V^{-1} s^{-1}]	$\omega_p{}^2$ [THz]
1 : 1	2 ps	−0.93	27.0	27.3	1.9	29.5
	500 ps	−0.85	42.8	43.3	6.5	13.7
1 : 4	2 ps	−0.86	32.0	32.4	5.5	14.4
	500 ps	−0.88	43.6	44.1	5.3	19.1

presence of pBTTT-rich domains, we performed the same experiments with excitation at 400 nm on a partially phase-separated 1 : 1 blend, processed with the additive Me7 (see Methods). This leads to the formation of a three-phase system (with co-crystalline regions, PCBM-rich and polymer-rich domains, Fig. S1d†), and to enhanced solar cell efficiency compared to the one-phase 1 : 1 blend.[25] In our previous investigations of such three-phase systems, we have shown that gCR is reduced compared to the one-phase 1 : 1 blend (49% instead of 87%), that the co-crystalline phase is preferentially excited at 400 nm, and that holes from the intermixed regions move to the polymer-rich domains on an extremely fast, 200 fs time scale.[26] The solid line in Fig. 4 shows the THz absorption time trace, the dashed line shows the TA dynamics, while the black diamonds show the data extracted from DSM fits at four pump–probe delays: 2, 5, 90 and 500 ps, respectively. We find a slight rise in THz photoconductivity on the first 100 ps followed by a rather constant conductivity (Fig. 4). This is in contrast to the TA and DSM population dynamics that show a decay due to gCR, indicating that changes in the effective mobility after excitation have a strong influence on the THz dynamics.

Fit parameters from the DSM to the frequency-dependent photoconductivities in Fig. 5 are given in Table 2. Compared to the 1 : 1 and 1 : 4 blends, the THz mobility at the 2 ps time delay is higher in the 1 : 1 blend with Me7. Since the latter is in principle comparable to the 1 : 4 blend, but with additional pBTTT-rich regions, this difference must stem from this additional third phase. Indeed, holes are already expected to have reached this phase within 2 ps, explaining the high THz mobility. At subsequent time delays, the THz mobility slightly decreases, which might be due to traps formed by the Me7 additive, in agreement with our previous observations using EDA spectroscopy.[26] On the other hand, there is an impressive increase in charge delocalization with time (as shown by the evolution of the c_1 parameter), which leads to very high effective mobilities after 90 ps, even higher than the ones found for the 1 : 4 blend. The smaller imaginary part contribution to the conductivity spectra of the Me7 blend also clearly indicates a more efficient delocalization of charges. Overall, for the three-phase system produced with Me7, we find the charge density to decay less prominently than in the one-phase 1 : 1 blend, while observing mobilities comparable or higher than those of the 1 : 4 blend with PCBM-rich regions. Separating the long-lived charges (which do not undergo gCR) into neat fullerene-rich and polymer-rich phases thus has a very beneficial impact on their short-range mobility and delocalization. Together with the favourable energy cascade in the three-phase system produced with Me7, this contributes to the superior device performance

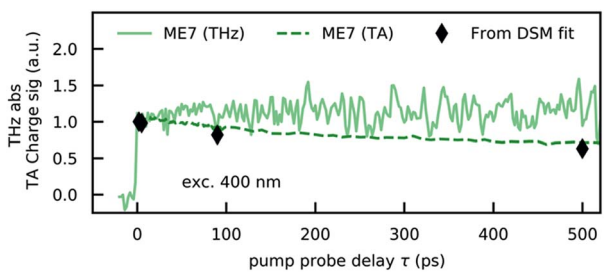

Fig. 4 THz photoconductivity dynamics on the three-phase 1 : 1 blend with Me7, comprising co-crystalline, PCBM-rich and polymer-rich regions, excited with optical pump pulses at 400 nm. Solid lines show the absorption of the maximum THz field at varied pump–probe delays. Dashed lines show the charge population extracted from TA measurements. Black diamonds in the lower panel show the normalized charge density extracted from fits of the Drude–Smith-model to frequency-dependent photoconductivity spectra at various pump–probe time delays.

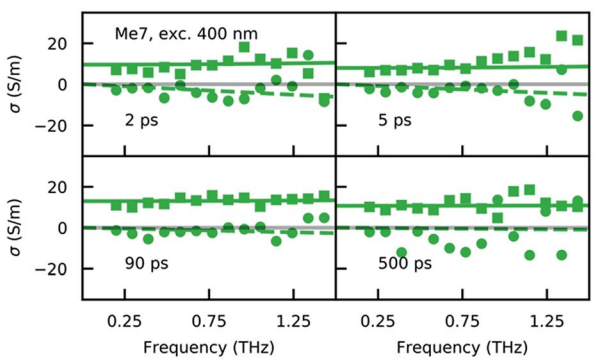

Fig. 5 Complex photoconductivity spectra (squares for the real part and circles for the imaginary part) and Drude–Smith-model fits (solid lines) for the partially phase-separated 1 : 1 blend with Me7 at 400 nm excitation at pump–probe delays of +2 ps, +5 ps, +90 ps and +500 ps.

Table 2 Fit results of the modified DSM on the frequency-dependent photoconductivity data on the three-phase system with Me7

Me7, 400 nm	c_1	τ [fs]	μ_{THz} [cm^2 V^{-1} s^{-1}]	μ_{eff} [cm^2 V^{-1} s^{-1}]	$\omega_p{}^2$ [THz]
2 ps	−0.91	47.5	48.1	4.3	16.0
5 ps	−0.92	43.7	44.2	3.5	15.7
90 ps	−0.80	44.1	44.6	8.9	13.1
500 ps	−0.72	41.5	42.0	11.8	10.1

of this ternary blend compared to the one-phase one, that is dominated by the co-crystalline phase.[25] High delocalization is also a sign of long-range free charge transport at high THz mobility, leading to the high effective mobility which is crucial for efficient device performance.[44,45]

Short-range mobility and charge separation

As mentioned in the introduction, the short-range charge mobility in polymer:fullerene blends plays an important role in helping the dissociation of geminate electron–hole pairs from charge transfer (CT) states.[8] In all blends, we find high THz mobilities at short times (around 30–40 cm^2 V^{-1} s^{-1}). This assists the efficient charge separation, due to a higher rate of CT state splitting with higher scattering times.[8] Since this more ballistic and very local THz mobility is expected to be high in all conjugated systems, it does however not allow to differentiate samples with high or low gCR loss. We therefore suggest that the short-range effective mobility, which includes both the THz mobility and hopping of the charges between localized sites, might be a better parameter to evaluate how much the mobility helps the separation of charges. Indeed, with 400 nm excitation, the early μ_{eff} (at 2 ps) of 1.9, 4.3 and 5.5 cm^2 V^{-1} s^{-1} for the 1 : 1 blend, the 1 : 1 blend with Me7 and the 1 : 4 blend, respectively, follows the trend of reduced gCR and higher solar cell efficiency. Moreover, the higher effective mobility with 400 nm compared to 540 nm excitation agrees with the 12% higher yield of free charges in the 1 : 1 blend at 400 nm (Fig. S3†). It somewhat contradicts the reported observation that OPV solar cell efficiency is generally independent on the excitation energy, yielding flat internal quantum efficiency (IQE) spectra.[46] Nevertheless, IQE curves are typically reported on a logarithmic scale and do not reflect the small changes in gCR that we see here. Kinetic Monte Carlo simulations have shown that for a reasonable CT state lifetime of 10 ns, the initial short-range mobility defines the effectiveness of charge separation for a given size of the intermixed region.[8] In our case, the co-crystalline domain size is expected to be within the typical 2–15 nm range of the intermixed phase in bulk heterojunctions,[27,47] and therefore the required short-range mobility must be on the order of 2–7 cm^2 V^{-1} s^{-1}, which is clearly achieved in the more efficient blends. In addition to the high short-range mobility, other factors such as the presence of an energy cascade due to the co-existence of phase-pure and intermixed regions, influence the charge separation. An energy cascade is only present here in the Me7 and 1 : 4 blends, also explaining the reduced gCR in these systems. We find consistently increased effective mobilities at long times for all blends, showing that, even if charges with different properties are initially generated, only the ones exhibiting large short-range mobility prevail and survive gCR.

Comparison to EDA transport measurements

Finally, we compare our findings using THz spectroscopy to the ones we previously reported for the pBTTT:PCBM systems using EDA spectroscopy, in order to highlight the complementarity of the two techniques. In EDA, the sample in solar cell device configuration is subjected to a static electric field and the distance between the photogenerated electron and hole is deduced from the residual electric field between the electrodes as the charges move apart.[26] Fig. 6 shows the average electron–hole distance l and the associated EDA mobility from:

$$\mu_{EDA} = \frac{d}{U}\frac{\partial}{\partial t}l,$$

where d is the device thickness and U the applied voltage.[48] For the average electron–hole distance, we find a higher initial separation within the 1 : 1 blend treated with Me7, consistent with the high initial THz mobility and the ultrafast transport of holes into the neat pBTTT regions. At long time delays, the greatest electron–hole separation is achieved in the 1 : 4 blend (where the electrons travel in the neat fullerene clusters), while the weakest separation occurs in the one-phase 1 : 1 blend (in

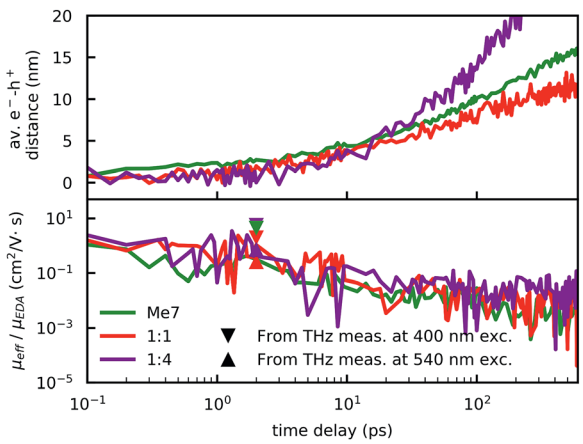

Fig. 6 Average electron–hole distance at various times after photoexcitation probed with EDA spectroscopy (top) and the extracted EDA mobilities (bottom). The excitation wavelength was 540 nm for the 1 : 1 and 1 : 4 blends, and 390 nm for the Me7 sample. Triangles show the measured effective THz mobilities at a 2 ps pump–probe delay for excitation with 400 nm (triangle down) and excitation with 540 nm (triangle up).

the absence of fullerene- and polymer-rich regions). The three-phase blend processed with Me7 shows an intermediate electron–hole separation at long time delays (in spite of the presence of neat pBTTT and PCBM regions), which we have attributed to traps formed by the Me7 additive.[26] When considering the evolution of the EDA mobility with time, there is a continuous decrease of the mobility over four orders of magnitude within 1 ns. This is due to the dispersive nature of the transport, since EDA probes increasingly long distances at longer time delays.[9] In contrast, THz spectroscopy always probes the short-range mobility of the charges in the region of the blend where they are found at a given pump–probe delay.

In Fig. 6, triangles depict the effective mobilities deduced from the THz photoconductivity 2 ps after photoexcitation. It is comparable to the EDA mobility at the same time delay, at which the electron–hole separation of a few nanometres indicates that a similar transport distance is probed. The fact that the THz mobility is slightly higher than the EDA mobility can be attributed to the different nature of the electric field in which the charges drift. With the EDA technique, the applied field of 600 kV cm^{-1} is constant throughout the migration of charges and is applied unidirectionally between external electrodes, so that only the projection of the electron–hole separation in this direction is seen (the actual motion of the charges might be longer). The high initial mobility reduces significantly due encounters of energetic boundaries as the charges travel larger distances. On the other hand, with the THz technology, the applied field oscillates and changes polarity before a charge reaches any energetic boundaries, leading to a more short-range nature of the mobility. In both experiments, the earliest times after photoexcitation at which we access mobilities are on the order of a few picoseconds. By that time ultrafast processes, which dominate the first 1000 fs, such as the ballistic transport regime for the first few fs, followed by transient localization during the first ps, are overtaken by diffusive transport.[43] Here, using THz spectroscopy, we are able to investigate this diffusive transport on length scales of 1 nm, giving an intrinsic mobility measurement which is impossible to achieve with other technologies, be it contacted or non-contacted.

Conclusion

We present here optical-pump-THz-probe measurements of pBTTT:PCBM blends with controlled phase morphologies. We compare samples containing only one-phase, the co-crystalline phase, to samples with a two-phase morphology comprised of co-crystalline and fullerene-rich phases, as well as samples containing co-crystalline and both PCBM-rich and pBTTT-rich regions. We show that the local phase-morphology governs charge separation and charge mobility. By investigating the THz photoconductivity dynamics for these three systems at low excitation fluences, we can directly compare them to transient absorption measurements, in order to distinguish between the evolution of the charge density and their short-range mobility. Looking closely at the frequency-dependent photoconductivity shortly after excitation and 500 ps later, we then further investigate the impact of local morphology on the THz mobility (mainly ballistic) and the short-range effective mobility (including localization effects, but not grain boundaries and electrodes), obtained using the Drude–Smith model. High THz mobility (around 30–40 $cm^2 V^{-1} s^{-1}$) is found in all systems and at different excitation energies, while significant differences in the effective mobility at short times can be correlated to efficient separation of geminate electron–hole pairs. Efficient systems typically have >2 $cm^2 V^{-1} s^{-1}$ effective mobility (at 2 ps after photoexcitation), as well as co-existing co-crystalline and fullerene- and/or polymer-rich regions leading to favourable energy cascades. We generally notice that charges surviving geminate recombination are the ones having a higher effective mobility. Moreover, migration of charges from the co-crystalline into the fullerene-/polymer-rich regions at long time delays (500 ps) increases their delocalization and effective mobility. The presence of fullerene-/polymer-rich regions thus not only influences the device performance by increasing the lifetime of photogenerated charges (by reducing geminate recombination), but also provides the necessary charge delocalization for effective transport within local phases. Using THz spectroscopy at low excitation densities provides a tool in the study of organic semiconductors that allows to understand how the phase morphology of OPV blends needs to be tuned in order to optimize the short-range mobility of the charges for best charge separation and transport.

Conflicts of interest

There are no conflicts to declare.

Acknowledgements

PK, DT, MC and NB thank the Swiss National Science Foundation (grant PP00P2_150536 and National Competence Center for Research NCCR-MUST: Molecular Ultrafast Science and Technology), as well as the University of Bern for financial support. NS and NB thank the EC for funding *via* the Marie Skłodowska-Curie Actions Innovative Training Network "H2020-MSCAITN-2014 INFORM – 675867" that enabled many meetings and discussions between all authors.

References

1 J. You, L. Dou, K. Yoshimura, T. Kato, K. Ohya, T. Moriarty, K. Emery, C.-C. Chen, J. Gao, G. Li and Y. Yang, *Nat. Commun.*, 2013, **4**, 1446.
2 J. Hou, O. Inganäs, R. H. Friend and F. Gao, *Nat. Mater.*, 2018, **17**, 119.
3 S. Günes, H. Neugebauer and N. S. Sariciftci, *Chem. Rev.*, 2007, **107**, 1324–1338.
4 S. R. Forrest, *Nature*, 2004, **428**, 911.
5 N. S. Lewis, *Science*, 2007, **315**, 798–801.
6 P. Bøggild, D. M. Mackenzie, P. R. Whelan, D. H. Petersen, J. D. Buron, A. Zurutuza, J. Gallop, L. Hao and P. U. Jepsen, *2D Mater.*, 2017, **4**, 042003.
7 B. Philippa, M. Stolterfoht, P. L. Burn, G. Juška, P. Meredith, R. D. White and A. Pivrikas, *Sci. Rep.*, 2014, **4**, 5695.

8 T. M. Burke and M. D. McGehee, *Adv. Mater.*, 2014, **26**, 1923–1928.
9 M. Armantas, P. Vytenis, D. Andrius, G. Vidmantas, I. Olle and K. Martijn, *Adv. Funct. Mater.*, 2014, **24**, 4507–4514.
10 F. Steiner, C. Poelking, D. Niedzialek, D. Andrienko and J. Nelson, *Phys. Chem. Chem. Phys.*, 2017, **19**, 10854–10862.
11 R. Noriega, J. Rivnay, K. Vandewal, F. P. V. Koch, N. Stingelin, P. Smith, M. F. Toney and A. Salleo, *Nat. Mater.*, 2013, **12**, 1038–1044.
12 R. Noriega, *Macromol. Rapid Commun.*, 2018, 1800096.
13 J. C. Brauer, M. Causa' and N. Banerji, in *Nanostructured Materials for Type III Photovoltaics*, The Royal Society of Chemistry, 2018, pp. 226–267.
14 I. Ramirez, M. Causa', Y. Zhong, N. Banerji and M. Riede, *Adv. Energy Mater.*, 2018, 1703551.
15 V. Abramavičius, D. A. Vithanage, A. Devižis, Y. Infahsaeng, A. Bruno, S. Foster, P. E. Keivanidis, D. Abramavičius, J. Nelson, A. Yartsev, V. Sundström and V. Gulbinas, *Phys. Chem. Chem. Phys.*, 2014, **16**, 2686–2692.
16 E. Hendry, J. M. Schins, L. P. Candeias, L. D. A. Siebbeles and M. Bonn, *Phys. Rev. Lett.*, 2004, **92**, 196601.
17 E. Hendry, M. Koeberg, J. M. Schins, L. D. A. Siebbeles and M. Bonn, *Chem. Phys. Lett.*, 2006, **432**, 441–445.
18 P. D. Cunningham and L. M. Hayden, *J. Phys. Chem. C*, 2008, **112**, 7928–7935.
19 E. Hendry, M. Koeberg, J. M. Schins, H. K. Nienhuys, V. Sundström, L. D. A. Siebbeles and M. Bonn, *Phys. Rev. B: Condens. Matter Mater. Phys.*, 2005, **71**, 125201.
20 S. Meng-Ju, J. A. Bartelt, T. M. Burke, A. Salleo, M. D. McGehee and A. M. Lindenberg, *Adv. Electron. Mater.*, 2016, **2**, 1500351.
21 C. S. Ponseca, H. Němec, N. Vukmirović, S. Fusco, E. Wang, M. R. Andersson, P. Chabera, A. Yartsev and V. Sundström, *J. Phys. Chem. Lett.*, 2012, **3**, 2442–2446.
22 C. S. Ponseca, A. Yartsev, E. Wang, M. R. Andersson, D. Vithanage and V. Sundström, *J. Am. Chem. Soc.*, 2012, **134**, 11836–11839.
23 P. Parkinson, J. Lloyd-Hughes, M. B. Johnston and L. M. Herz, *Phys. Rev. B: Condens. Matter Mater. Phys.*, 2008, **78**, 115321.
24 A. Mayer, M. F. Toney, S. R. Scully, J. Rivnay, C. J. Brabec, M. Scharber, M. Koppe, M. Heeney, I. McCulloch and M. D. McGehee, *Adv. Funct. Mater.*, 2009, **19**, 1173–1179.
25 E. Buchaca-Domingo, A. J. Ferguson, F. C. Jamieson, T. McCarthy-Ward, S. Shoaee, J. R. Tumbleston, O. G. Reid, L. Yu, M. B. Madec, M. Pfannmöller, F. Hermerschmidt, R. R. Schröder, S. E. Watkins, N. Kopidakis, G. Portale, A. Amassian, M. Heeney, H. Ade, G. Rumbles, J. R. Durrant and N. Stingelin, *Mater. Horiz.*, 2014, **1**, 270–279.
26 M. Causa', J. De Jonghe-Risse, M. Scarongella, J. C. Brauer, E. Buchaca-Domingo, J.-E. Moser, N. Stingelin and N. Banerji, *Nat. Commun.*, 2016, **7**, 12556.
27 A. A. Paraecattil and N. Banerji, *J. Am. Chem. Soc.*, 2014, **136**, 1472–1482.
28 M. Scarongella, A. A. Paraecattil, E. Buchaca-Domingo, J. D. Douglas, S. Beaupre, T. McCarthy-Ward, M. Heeney, J. E. Moser, M. Leclerc, J. M. J. Frechet, N. Stingelin and N. Banerji, *J. Mater. Chem. A*, 2014, **2**, 6218–6230.
29 C. Bauer, J. Teuscher, J. C. Brauer, A. Punzi, A. Marchioro, E. Ghadiri, J. De Jonghe, M. Wielopolski, N. Banerji and J.-E. Moser, *Chimia*, 2011, **65**, 704–709.
30 A. Devižis, A. Serbenta, K. Meerholz, D. Hertel and V. Gulbinas, *Phys. Rev. Lett.*, 2009, **103**, 027404.
31 I. McCulloch, M. Heeney, C. Bailey, K. Genevicius, I. MacDonald, M. Shkunov, D. Sparrowe, S. Tierney, R. Wagner, W. Zhang, M. L. Chabinyc, R. J. Kline, M. D. McGehee and M. F. Toney, *Nat. Mater.*, 2006, **5**, 328.
32 M. Scarongella, J. De Jonghe-Risse, E. Buchaca-Domingo, M. Causa', Z. Fei, M. Heeney, J.-E. Moser, N. Stingelin and N. Banerji, *J. Am. Chem. Soc.*, 2015, **137**, 2908–2918.
33 D. W. Gehrig, I. A. Howard, S. Sweetnam, T. M. Burke, M. D. McGehee and F. Laquai, *Macromol. Rapid Commun.*, 2015, **36**, 1054–1060.
34 F. C. Jamieson, E. B. Domingo, T. McCarthy-Ward, M. Heeney, N. Stingelin and J. R. Durrant, *Chem. Sci.*, 2012, **3**, 485–492.
35 X. Ai, M. C. Beard, K. P. Knutsen, S. E. Shaheen, G. Rumbles and R. J. Ellingson, *J. Phys. Chem. B*, 2006, **110**, 25462–25471.
36 M. Causa', I. Ramirez, J. F. Martinez Hardigree, M. Riede and N. Banerji, *J. Phys. Chem. Lett.*, 2018, **9**, 1885–1892.
37 R. Ulbricht, E. Hendry, J. Shan, T. F. Heinz and M. Bonn, *Rev. Mod. Phys.*, 2011, **83**, 543–586.
38 Z. Jin, D. Gehrig, C. Dyer-Smith, E. J. Heilweil, F. Laquai, M. Bonn and D. Turchinovich, *J. Phys. Chem. Lett.*, 2014, **5**, 3662–3668.
39 J. E. Northrup, *Phys. Rev. B: Condens. Matter Mater. Phys.*, 2007, **76**, 245202.
40 N. Banerji, *J. Mater. Chem. C*, 2013, **1**, 3052–3066.
41 I. Hwang and G. D. Scholes, *Chem. Mater.*, 2011, **23**, 610–620.
42 W. Barford, I. Boczarow and T. Wharram, *J. Phys. Chem. A*, 2011, **115**, 9111–9119.
43 F. Simone, M. Didier and C. Sergio, *Adv. Funct. Mater.*, 2016, **26**, 2292–2315.
44 N. Shin, L. J. Richter, A. A. Herzing, R. J. Kline and D. M. DeLongchamp, *Adv. Energy Mater.*, 2013, **3**, 938–948.
45 Y. Gu, C. Wang and T. P. Russell, *Adv. Energy Mater.*, 2012, **2**, 683–690.
46 K. Vandewal, S. Albrecht, E. T. Hoke, K. R. Graham, J. Widmer, J. D. Douglas, M. Schubert, W. R. Mateker, J. T. Bloking, G. F. Burkhard, A. Sellinger, J. M. J. Fréchet, A. Amassian, M. K. Riede, M. D. McGehee, D. Neher and A. Salleo, *Nat. Mater.*, 2013, **13**, 63.
47 A. Serbenta, O. V. Kozlov, G. Portale, P. H. M. van Loosdrecht and M. S. Pshenichnikov, *Sci. Rep.*, 2016, **6**, 36236.
48 V. Pranculis, Y. Infahsaeng, Z. Tang, A. Devižis, D. A. Vithanage, C. S. Ponseca, O. Inganäs, A. P. Yartsev, V. Gulbinas and V. Sundström, *J. Am. Chem. Soc.*, 2014, **136**, 11331–11338.